33RD CONGRESS
OF THE INTERNATIONAL COUNCIL
OF THE AERONAUTICAL SCIENCES
STOCKHOLM, SWEDEN, 4-9 SEPTEMBER, 2022

ICAS 2022 SWEDEN

HYBRID ELECTRIC PROPULSION SYSTEM OPTIMIZATION FOR A COMMUTER AIRCRAFT

Petter Krus[1], Ingo Staack[1] & Amir A. M. Oliveira[2]

[1]Linköping University, Sweden
[2]Federal University of Santa Catarina, Brazil

Abstract

This paper shows how simulation-based optimization can be used to investigate the impact of technology development on the feasibility and performance of electric aircraft. This work investigates the design of an electric/hydrogen-powered commuter aircraft (certified according to CS/FAR 23) based on a dynamic mission simulation including a 6DOF flight dynamics aircraft model. The electric/hydrogen hybrid propulsion system is being optimized to realize a design missions of $500\,\mathrm{km}$ and $1000\,\mathrm{km}$, respectively, based on present technology levels with a scenario with technology improvement of batteries and fuel cells. By the optimization-based sizing of the propulsion train components, automated morphological and topological changes on the propulsion system are realized. The results cover a spectrum from pure electric to pure hydrogen fuel cell aircraft including all possible hybrid solutions in between. In this way, simulation-based optimization is demonstrated also for its use for concept selection and system architecture optimization.

Keywords: electric propulsion, fuel cell, hydrogen, model-based optimization, green aviation

1. Background

Battery-electric aircraft suffer from a high empty weight (OEW) fraction and a low payload fraction. Even with this design characteristics, the mission range is extremely limited, see [16], which hampers a practicable and profitable use as commuter aircraft with the current (year 2022) battery performance properties. While heading towards a sustainable air transportation until 2045 (in Sweden []), other propulsion methods beside full-electric battery aircraft have to be considered, ranging from liquid fuel types (e-fuels, *sustainable aviation fuel* (SAF), *bio-aviation fuel* (BAF)) or gaseous fuels like Methane (CH_4), natural gas (a mixture formed mainly by CH_4), or hydrogen (H_2). The latter category may be stored in gas phase at high pressures and/or in liquid phase at cryogenic temperatures (e.g., liquefied natural gas (LNG) or liquid hydrogen). Hydrogen (H_2) seems to become a prominent successor for nowadays fossil-fuel-based aviation propulsion due to various characteristics such as:

- best specific energy among all liquid and gas fuels ($142\,\mathrm{MJ/kg}$),
- various storing alternatives: gaseous (pressurized), liquid (cryogenic), or chemical storages,
- versatile use as fuel: compatible with heat engines and fuel cells,
- availability: ramping-up infrastructure (in Sweden: due to the "hydrogenization" of the energy-intensive industry, e.g., iron/steel, chemical, concrete; in Europe: existing pipeline infrastructure and eventually synergies with heavy road transportation; in Brazil: the production of green hydrogen from renewable sources is expected to increase exponentially in the next years, mainly destined to export [3], in world: decarbonization of carbon intensive sectors as steel, cement, chemicals, long-haul transport and maritime shipping will provide additional synergies [5]) ,

- hydrogen source: various ways of production (sustainable/fossil-based): from electrolysis powered by solar, wind power, nuclear, fossil fuel electricity (named as green, yellow, and blue hydrogen), from reforming of natural gas (*steam methane reforming* (SMR)), fossil fuels and biofuels (NH_3), etc..

Due to the increasing performance of batteries, a combination of both power sources seems promising. One reason is that it can adapt and benefit from the gradual improvement of technologies, i.e. in batteries, eventually making the fuel cell and hydrogen storage redundant at least for shorter missions. Such combinations of fuel cells and batteries were investigated by Kady [7] among others. In this paper however, more detailed dynamic (cyber-physical) simulation models are used to enable a simulation-based optimization process of the propulsion system architecture.

2. Aircraft Concept

The commuter aircraft in this study is to be conform with the CS/FAR-23 regulations. The basic limitations of this aircraft category are:

- max. 19 passengers, and
- 19000 lb (8618 kg) maximum take-off weight.

While the passenger limit is motivated by safety arguments (absence of cabin crew, aircraft reliability, lower operational requirements compared to CS/FAR 25), the weight limit is not as clearly coupled to e.g., safety criteria and may be negotiable and subject to change in future releases (see even the development of new certification standard for *urban air mobility* (UAM) vehicles).
The aircraft concept studied here is very straightforward, with a twin motor/propeller configuration. However, increasing the number of motors, or changing the concept of the aircraft, can change the characteristics of the airplane, but it is only the effect on lift-to-drag (L/D) (which is here set to 20 at cruise) and the propulsive efficiency η_{total} that will have a significant influence on range. I.e., an increase of 10% of the lift-to-drag ratio, would just increase the range by the same amount, and the same goes for propulsive technology. The structural efficiency can be translated into an increase in payload or battery mass with the (CS/FAR 23) weight limit active. The energy carrier, on the other hand, can change range by orders of magnitude.
The aircraft modelled here has a lift-to-drag ratio of about 20 at cruise speed which is high compared to today´s aircraft but feasible at the lower speeds of such an aircraft (more comparable to piston engine-propeller or turboprop airplanes).

3. Propulsion System

The propulsion system consists of two electric motors with one propeller each driving through a gearbox. The energy is provided by the battery and/or the hydrogen-fed fuel cell, see Fig. 1. Following the notation by [6], it is a serial hybrid type of a dual-energy propulsion and power systems (DESPPS) architecture with the ability to recharge the battery with the electricity from the fuel cell in flight.

3.1 Fuel Cell

In a fuel cell, chemical energy is converted directly into electric energy. A *proton exchange membrane fuel cell* (PEMFC) operates with hydrogen and oxygen (or air) producing water. The electrochemical reactions at the electrode may be represented as:

$$\begin{aligned} \mathrm{H_2(g)} &\longrightarrow 2\,\mathrm{H^+} + 2\,\mathrm{e^-} && , \quad \text{at the anode,} \\ \tfrac{1}{2}\,\mathrm{O_2\,(g)} + 2\,\mathrm{H^+} + 2\,\mathrm{e^-} &\longrightarrow \mathrm{H_2O\,(l)} && , \quad \text{at the cathode,} \\ \mathrm{H_2(g)} + \tfrac{1}{2}\,\mathrm{O_2(g)} &\longrightarrow \mathrm{H_2O\,(l)} && , \quad \text{overall.} \end{aligned} \tag{1}$$

Fuel cell simulation abstraction and modelling approaches at a level that is relevant here can be found in [1], [2], [12], [14], and [11]. These are models that include fundamental (physical and chemical) aspects and provide a fidelity that suits the system simulations at conceptual design stage. Modelling of fuel cells for aircraft is presented in [15]. The characteristic behaviour of the power produced by a fuel cell is shown in Fig. 2. It is an electrical power source with an internal electrical resistance,

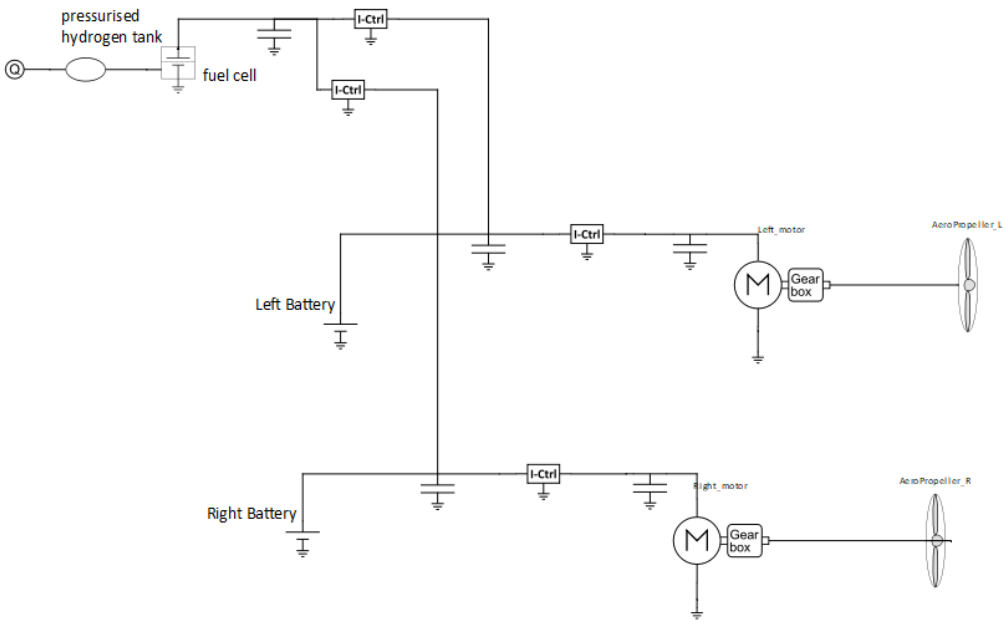

Figure 1 – Electric power system model used for the optimization. The two motors are supplied through two batteries and one fuel cell.

therefore, comparable to solar cells or batteries in this aspect. As clearly visible in Fig. 2, the sizing of the fuel cell is a compromise between weight and size (high power loading) and efficiency (low power loading). Efficiency is a direct function of output voltage. With no losses at zero current. Hence the efficiency at the peak power at $52.5A$ is about $\eta_{FC} = 0.65/1.22 = 0.53$

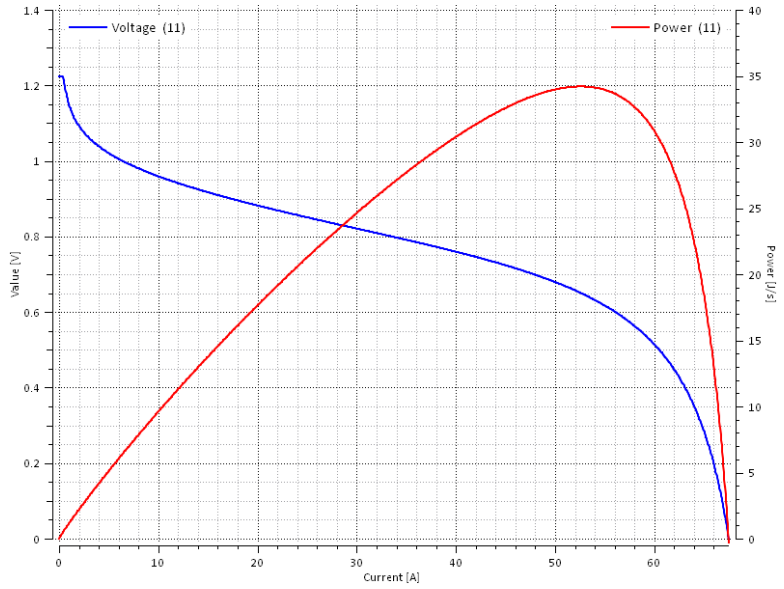

Figure 2 – The characteristics of one fuel cell. The fuel cell voltage (blue) as a function of current and the output power (red). The fuel cell area $A = 0.01\mathrm{m}^2$. Other values are from Table 1.

The PEMFC voltage is given as a contribution of several factors. At open circuit,

$$u_{fco} = \mathrm{lowLimit}\left[u_{nernst} - u_{act} - u_{con}, 0\right], \tag{2}$$

where u_{nernst} is the ideal (Nernst) potential, u_{act} is the activation overpotential, and u_{con} is the concentration (mass transfer) potential drop.
When the cell is generating power, there is an additional internal potential drop due to internal elec-

trical resistances, and

$$u_{fcr} = \text{lowLimit}\left[u_{nernst} - u_{act} - u_{con} - u_{ohmic}, 0\right], \tag{3}$$

where u_{ohmic} is the voltage loss due to internal electrical resistances.
Nerst equation provides the equilibrium (reversible, open circuit) voltage of the fuel cell. Assuming a reference state at T_{ref}, p_0, it is given by

$$u_{nernst} = \frac{\Delta G}{2F} + \frac{\Delta S}{2F}\left(T - T_{ref}\right) + \frac{RT}{2F}\ln\left(\frac{P_{\mathrm{H_2}}\sqrt{P_{\mathrm{O_2}}}}{P_{\mathrm{H_2O}}}\frac{1}{\sqrt{p_0}}\right) \tag{4}$$

where $F = 96485$ C is Faraday´s constant. The first and second terms are the thermodynamic free energy of reaction and entropy change of the reaction occurring at T. The last term is the entropic contribution due to the reaction quotient at the electrode surface.
The activation potential drop is the overvoltage needed to run the eletrochemical reactions at the surface of the electrodes. It is calculated from

$$u_{act} = \text{lowLimit}\left[u^*_{act}, 0\right], \tag{5}$$

where

$$u^*_{act} = \xi_1 + \xi_2 T + \xi_3 T \ln C_{\mathrm{O_2}} + \xi_4 T \ln\left(i^*_{fco}\right), \tag{6}$$

and

$$i^*_{fco} = \text{lowLimit}\left[i_{fco}, 10^{-30}\right], \tag{7}$$

where i_{fco} is the current. This is a semi-empirical model built from Tafel's equation [11]. Constant ξ_1 is the irreversible part of the open circuit voltage, which includes the effect of the exchange current density (it becomes the open circuit voltage when added to u_{nerst}). ξ_3 accounts for the O_2 solubility in the water layer at the cathode, ξ_4 is inversely proportional to the charge transfer coefficient α (the slope of the Tafel line) and ξ_2 is modeled as

$$\xi_2 = 0.00286 + 0.0002\ln(A) + 4.3\times10^{-5}\ln(C_{\mathrm{H_2}}), \tag{8}$$

where A is the fuel cell area, $C_{\mathrm{H_2}}$ is the hydrogen solubility in the water layer at the anode, assumed constant for a fully saturated triple line, and

$$C_{\mathrm{O_2}} = \frac{P_{\mathrm{O_2}}/P_0}{5.08\times10^6\cdot e^{-498/T}}. \tag{9}$$

The crossover potential drop accounts for fuel and electron crossover across the electrolyte. It is a minor effect with a larger importance in open circuit and is not included here.
The concentration (mass transfer) potential drop results from the mass transfer resistance of reactants from the bulk to the surface of the electrodes. Assuming that the partial pressure at the electrodes that result from the mass transfer limitations behaves linearly with the current, it is modeled as

$$u_{con} = -B\ \text{logA1}\left(\text{limit}\left[\frac{i_{fc}}{i_{fc,max}}, 0, 1.075\right]\right). \tag{10}$$

where B is a constant that depends on the fuel cell operating state.
The potential drop due to ohmic losses account for the electrical resistance of the electron flow along the electrical contacts and ion flow across the electrolyte:

$$u_{ohmic} = R_{ohmic} i_{fc}, \quad R_{ohmic} = \frac{\rho_M L}{A} \tag{11}$$

where L the thickness of the *membrane electrode assembly* (MEA), A is the fuel cell area and ρ_M is the membrane ionic resistivity modeled as

$$\rho_M = \frac{1.816\left\{1 + 0.03\ i_{fco}/A + 0.062(T/303)^2\left(\text{lowLimit}\left[i_{fco}/A, 0\right]\right)^{2.5}\right\}}{\left(\lambda - 0.634 - 3\ i_{fco}/A\right)\ \exp\left[4.18(T/303 - 1)\right]} \tag{12}$$

where λ is the nafion membrane average water content, i.e, the number of H_2O molecules per $SO_3{}^-$ group. It will be assumed constant here.
The fuel cell current is

$$i_{fc} = \text{onPositive}[p_{p1}]\ \text{onPositive}[T_{p1}]\ \frac{\left(u_{fc1} - \dfrac{u_{fc}}{n_{stack}}\right)}{R_{ohmic}}, \tag{13}$$

where n_{stack} is the number of fuel cells in the stack. The voltage u_{fc} is obtained from the external electric system. Equation 13 is limited using the onPositive function in order to prevent any current if there is no hydrogen pressure p_{p1}, i.e., when the tank is empty.
With these equations, the output from the fuel cell model can be calculated in the form of efficiency η_{fc}, electric power P_{fc}, hydrogen mass flow drawn from the tank q_{mp1}, entalpy flow from the hydrogen tank $\dot{E}$:

$$\begin{aligned} \eta_{fc} &= \frac{u_{fc}}{n_{stack}\ u_{nernst}} \\ P_{fc} &= u_{fc}\ i_{fc} \\ q_{mp1} &= -M_{\mathrm{H}_2}\ n_{stack}\ \frac{i_{fc}}{2F} \\ \dot{E}_{p1} &= q_{mp1}\ c_p\ T_{p1} \end{aligned} \tag{14}$$

where c_p is the hydrogen specific heat at T_{p1}, P_{p1}.
The mass m_{fc} of the fuel cell stack can be calculated from the ideal specific power k_{mF} (this is about twice the real specific power that includes losses),

$$m_{fc} = n_{stack}\ u_{nernst}\ \frac{J_{fc,max}}{k_{mF}}. \tag{15}$$

where $J_{fc,max}$ is the maximum current density.

3.2 Special functions used for modelling of the fuel cell

A number of functions has been defined in order to solve this system of differential algebraic equations in an efficient way.
The function

$$\text{LogA1}[x] = -\frac{1.3x}{1-(0.93x)^4} \tag{16}$$

is used as an approximation to the function

$$-\ln(1-x) \tag{17}$$

since the original equation has a derivative approaching infinity as x goes towards 1, making it numerically difficult to deal with. A comparison between the exact and approximate expressions is shown in Fig 3.

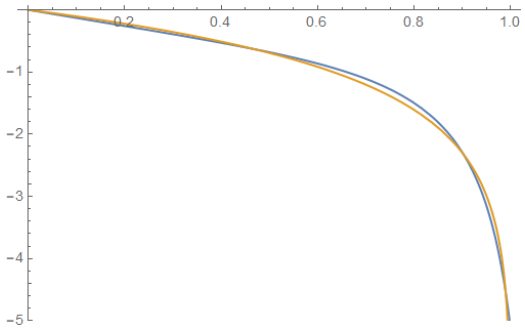

Figure 3 – Comparison between the function $\ln(1-x)$ (yellow) and LogA1(x) (blue).

The limitation function is defined as:

$$\text{limit}[x, xmin, xmax] = \begin{cases} x & \text{if } x_{min} < x < x_{max} \\ x_{min} & \text{if } x < x_{min} \\ x_{max} & \text{if } x > x_{max} \end{cases} \tag{18}$$

There is also the one sided limit function:

$$\text{lowLimit}[x, xmin] = \begin{cases} x & \text{if } x_{min} < x \\ x_{min} & \text{if } x < x_{min} \end{cases} \tag{19}$$

Finally, there is also the onPositive function:

$$\text{onPositive}[x] = \begin{cases} 1 & \text{if } x \geq 0 \\ 0 & \text{if } x < 0 \end{cases} \tag{20}$$

3.3 Parameters of the fuel cell

The following parameters are used:

Table 1 – Parameters and coefficients

$P_{\mathrm{H_2}}$	$1.476\,\mathrm{Atm}$	Hydrogen partial pressure
$P_{\mathrm{O_2}}$	$0.2095\,\mathrm{Atm}$	Oxygen partial pressure
$P_{\mathrm{H_2O}}$	$0.2095\,\mathrm{Atm}$	Water vapour partial pressure
R	$4124.2\,\mathrm{J/KgK}$	Gas constant for H_2
c_p	$14\,307.2\,\mathrm{J/KgK}$	Constant pressure specific heat
n_{stack}	1100	Number of cells in the stack
T	$323\,\mathrm{K}$	Temperature
T_{ref}	$298\,\mathrm{K}$	Reference temperature
L	$25 \times 10^{-6}\,\mathrm{m}$	Average thickness of the MEA
F	96485 C	Faraday's constant
ΔS	$0.85 \times 10^{-3}\,\mathrm{J/kmol - K}$	Change in entropy
ΔG	$228\,000.6\,\mathrm{J/kmol}$	Change in Gibbs free energy
B	$0.15\,\mathrm{V}$	Constant for the crossover potential drop
c_{H2}	0.2	H_2 solubility in the water layer at the anode
ξ_1	$-0.948\,\mathrm{V}$	Irreversible part of the open circuit voltage
ξ_3	$7.22 \times 10^{-5}\,\mathrm{V/K}$	Accounts for voltage drop due to O_2 solubility
ξ_4	$-1.064 \times 10^{-4}\,\mathrm{V/K}$	Slope of the Tafel line
λ	23.0	Membrane average water content
$J_{fc,max}$	$672. \times 10^{-3} \times 10^{4}\mathrm{A/m^2}$	Max current intensity
M_{H2}	$2.016 \times 10^{-3} \times 10^{4}\mathrm{kg/mol}$	Hydrogen molar weight
τ	$0.1\,\mathrm{kg/mol}$	Fuel cell time constant (mostly for numerics)

4. Modelling and Sizing

The approach used here to design an aircraft system is to use simulation based optimization. Here, a complete aircraft model is simulated over a design mission to achieve a high-fidelity behavioural model. Each simulation takes about 20 seconds which means that the hundreds of simulations needed for the optimization can be performed in a couple of hours on a desktop PC.

Aircraft Simulation Model is based on a *six degree of motion freedom* (6DOF) aircraft simulation model implemented in the simulation software HOPSAN. This is presented in [9] and [4]. To enable complex mission simulations, the simulation model also includes a flight control system and a mission control system. The autopilot controller receives the mission segment-specific operation (target) values from the mission controller.

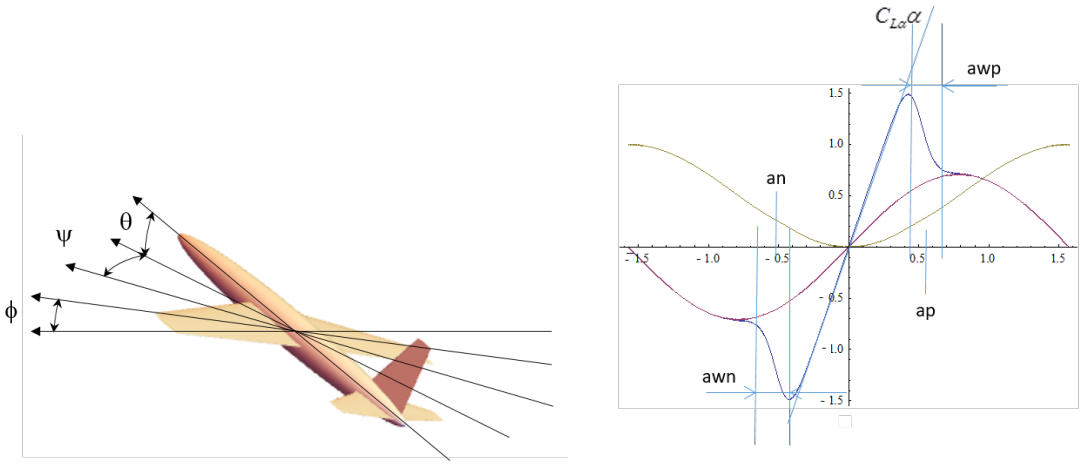

Figure 4 – 6DOF simulation model with non-linear aerodynamics used in the optimization.

Propulsion System is an complete sub-system including battery, fuel cell, electric motor, and the propeller models. The hydrogen storage is a high-pressure tank (800 bar) with a maximum fuel fraction of 6%. Furthermore, the battery voltage was set to 600 V. Because of this, the number of individual cells in the fuel cell stack was set to 1100 to ensure that the voltage is still above the battery voltage also at high currents, such as at maximum power. The exact voltage level have little consequence for the optimization in this study since weights are based on specific power, and hence voltage level does not really have an effect on the efficiency of the components.

The Mission There are two similar missions investigated in this paper. One is to fly 5000 km and the other is 10 000 km with a cruise altitude of 5000 m, with a cruise speed of 100 m/s. There are no reserves, so the practical range would be much smaller, but this is just to optimize the aircraft and see feasibility and the effects of different ranges and technology levels. The mission controller is implemented as an activity diagram from to the UML standard, see Fig.5.

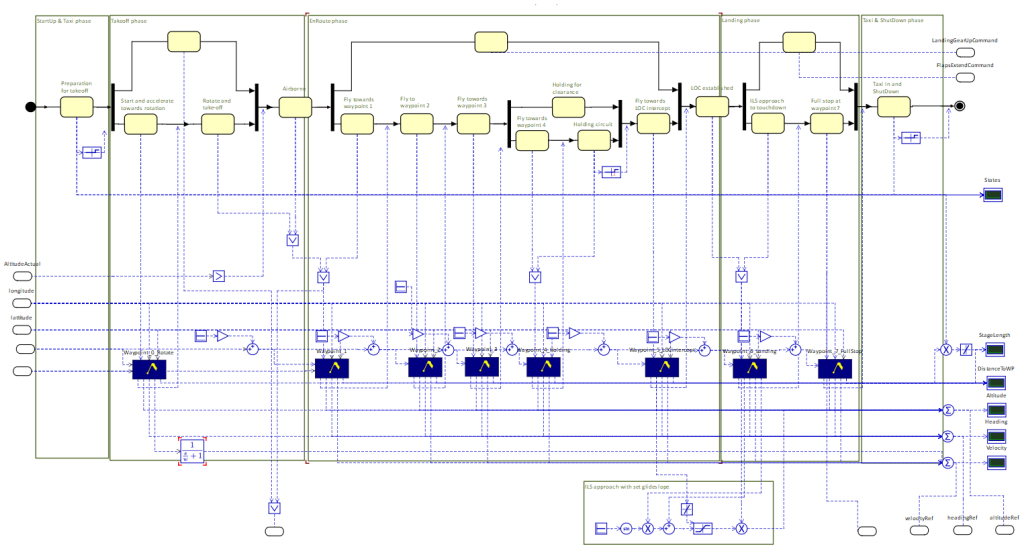

Figure 5 – The mission modelled as an UML activity diagram. E.g. when the aircraft model reach a waypoint it triggers the transition to another action element

5. System Optimization

Simulation-based optimization was introduced in [10], where a aircraft hydraulic servo was optimized simultaneously with respect to size parameters and control parameters, using a dynamic system

simulation model.Here a simulation model of the whole system is used to evaluate the performance at different parameter settings to eventually arrive at an optimal solution. By using a simulation model a high-fidelity behavioral model is obtained where the power produced and used by each component at any movement can be analysed.

5.1 Optimization Setup

Objective Function An objective function needs to be established to optimize the system. In this application, it is formulated as a single objective function that includes constraints as penalty functions. The primary objective is to minimize the system weight for the energy system, i.e., batteries, fuel cell, and hydrogen storage. The constraints are that the aircraft must land at the end of the simulation, and that the range requirement (500 km) has been fulfilled. The same optimization is then run but with the range set at (1000 km)
The objective function is formulated as a minimization problem with the following structure:

$$f_o = \sum_{i=1}^{n} \frac{f_i}{f_{0i}}^{\gamma_i} \tag{21}$$

The exponent γ typically has a value of two (but may be changed to increase or decrease the relative weight of a specific criteria) and the sign of positive if f_i is to be minimized and negative if it is to be maximized. f_{0i} is a target value or base line value.
The fist component is related to benefit and cost.

$$f_{01} = \frac{m_{pay0}}{m_{pay}} \left(1 - \kappa + \kappa \frac{E_{batt} + c_{H2} E_{H2}}{E_0}\right) \tag{22}$$

Here, m_{pay0} and E_0 are nominal values to make the function non-dimensional. c_{H2} is a factor that relates the cost of hydrogen energy to the cost of electricity. For these optimizations this factor was set to $c_{H2} =$, i.e. half an order of magnitude. This is a very uncertain value, but is is included to penalize the use of hydrogen compared to battery power. Furthermore, $= 0.2$. This gives a rather high weighting of energy cost and should favour the battery solution.

Optimization Setup The system has been optimized applying the COMPLEX-RF optimization algorithm on the above-described penalty function by changing the following design parameters:

- battery capacity (mass)
- Fuel cell area
- hydrogen storage (tank) volume
- Max reference current to fuel cell

Each change of a (component size) property has a direct influence on the component weight, therewith changing the OEW or MTOW of the aircraft and consequently contributing to the sizing of the aircraft (weight spiral effect). In order not to affect the sizing the total MTOW is kept constant by changing the payload instead.
The necessary (electric) control of the propulsion system balancing the fuel cell and battery load, and the recharging is realized by first controlling the motors. The batteries are directly connected to the motor controller. The fuel cell current is then controlled to give a maximum value during take-off and climb and are then controlled to charge the batteries as soon as the state-of-charge, SOC, goes below 0.2.
Optimizing the fuel cell parameters (cell area, number, and max current), battery size and hydrogen storage, it turns out that, with technology levels of about present day (2022), with a battery system energy density of ca. $200\,\mathrm{Wh/kg}$ and a fuel cell power density of about $1.0\,\mathrm{kW/kg}$, the resulting system has a small battery to give some boost power for the take-off and climb phase. The fuel cell provides a some increase of power during the climb segment and then take over propulsion completely in the cruise segment, see Fig. 5.

With a a cruise speed of $100\mathrm{km/h}$ and a cruise altitude of $5000\mathrm{m}$, the weight fraction made up by the system related to batteries, fuel cell and hydrogen storage represents 14.4% of the aircraft take-off weight. This makes it plausible to use it for a 19-passenger aircraft with a maximum take-off weight limit of $8618\mathrm{kg}$ ($19000\mathrm{lb}$), (CS/JAR 23 compliant) with a typical structural weight of ca. $3600\mathrm{kg}$.
The convergence of the optimization can be observed in Figure 6 by the increase of the information entropy over the 355 iterations(function evaluations) during one optimization run. An explanation of the significance of design entropy can be found in [8].

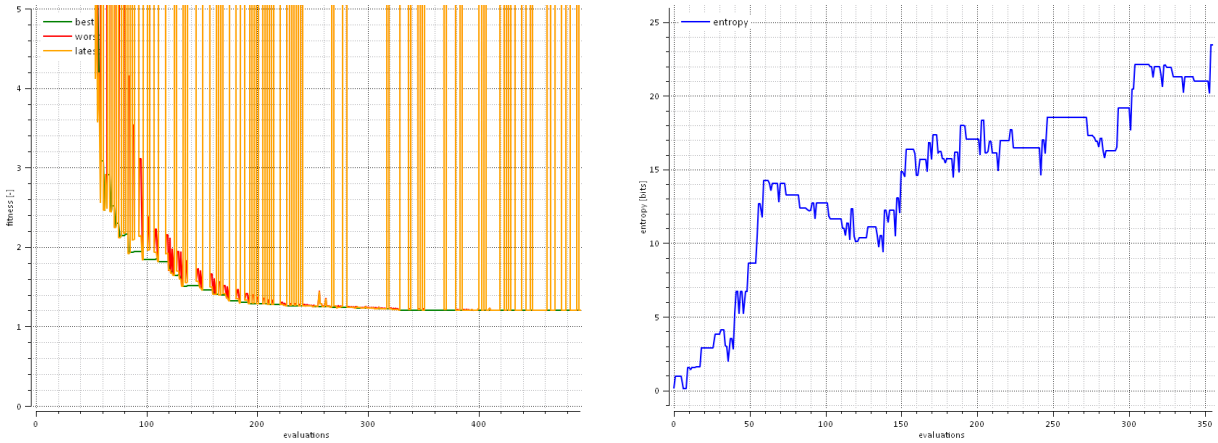

Figure 6 – The evolution of the objective function as a function of object function evaluations (simulations) left, and the estimated information entropy during optimization. It is a measure of the convergence of the optimization.

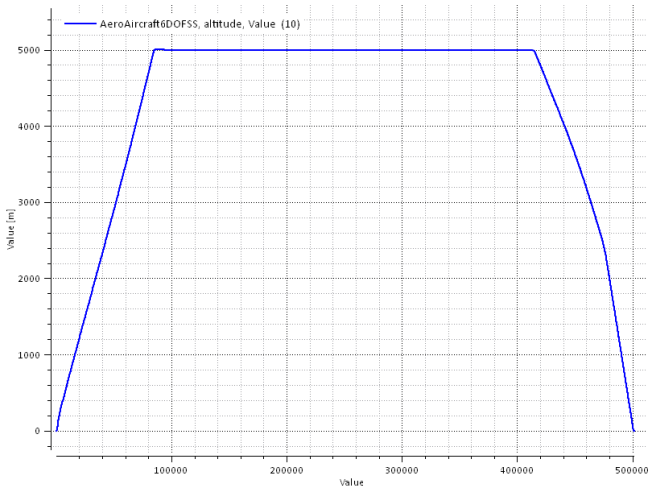

Figure 7 – Simulated mission. A $500\mathrm{km}$ mission with a cruise altitude of $5000\mathrm{m}$.

5.2 Optimization Results

The optimization gave the following results for the three cases:
shown in Table 2.

Table 2 – Optimization results

Case	I	II	III
Technology level	200 Wh/kg 1 kW/kg	200 Wh/kg 1 kW/kg	400 kg 2000 W/kg
Range	500 km	1000 km	1000 km
Total battery mass	640 kg	353 kg	351 kg
Hydrogen volume	0.587 m^3	1.071 m^3	0.906 m^3
Fuel cell area	0.189 m^2	0.246 m^2	0.232 m^2
Fuel cell max. ref current	*max*	*max*	668 A

Table 3 – Optimization weight results.

Case	I	II	III
Technology level	200 Wh/kg 1 kW/kg	200 Wh/kg 1 kW/kg	400 kg 2000 W/kg
Range	500 km	1000 km	1000 km
Payload mass	2332 kg	1903 kg	2514 kg
Battery mass	640 kg	353 kg	351 kg
Fuel cell mass	726 kg	946 kg	446 kg
Hydrogen initial mass	34 kg	62 kg	52.5 kg
Hydrogen storage initial mass	602 kg	1098 kg	928 kg
Fraction of storage and fuel cell	22.8%	27.8%	20.0%

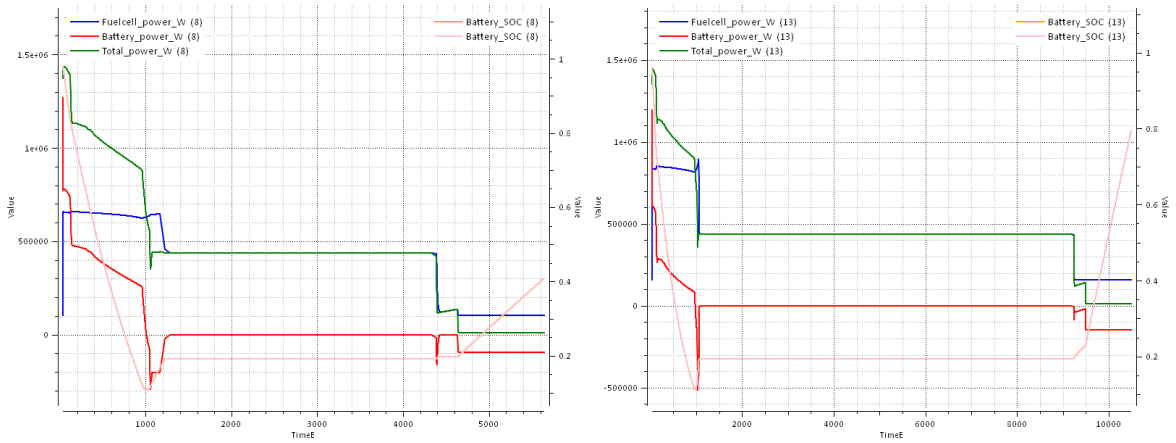

Figure 8 – Power from batteries, fuel cell and the total electric output for two different ranges. Left for case I and right for case II. Note the increase in maximum fuel cell power in the right case.

The electric power distribution over the mission after the optimization are shown in Fig. 8 and 9. It shows that the battery is used to boost the current during the take-off/climb stage. It is noteworthy to see that also the fuel cell is used to boost the electric power during the take-off and climb phase to a varying degree. There is a balance to strike here between the battery weight and the power density of the fuel cell as well as the efficiency of the fuel cell.
For case I it the increase the battery take most of the increase in power for the takeoff and climb phase. This is because the influence on efficiency of increasing the fuel cell size is not so significant when it comes at reducing the hydrogen storage, so here the battery with a marginally higher power density can be use full to boost the power.
In case II the fuel cell is larger, making the use of the battery much more marginal. Having a larger fuel cell increase the efficiency and therefore also reducing the consumption of hydrogen.
In case III the battery is increased, since it provides a cheaper energy and the power density has increased to make it have a smaller impact on weight. This is also the only case where the maximum reference current for the fuel cell had a real effect. This comes in a the takeoff and climb phase. For

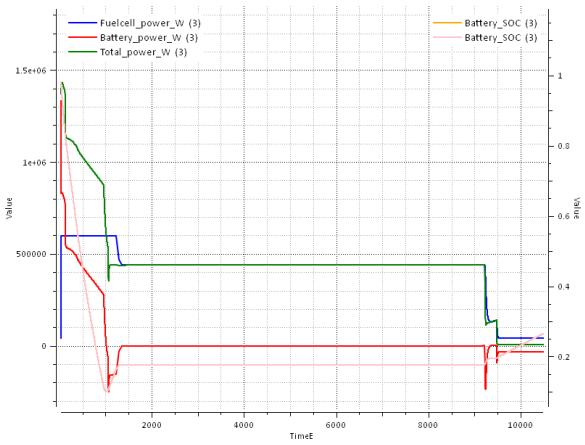

Figure 9 – Power from batteries, fuel cell and the total electric output for case III. Note the increased use of battery energy compared to case II.

the other two cases (I and II) the optimizer took it up to the maximum value of the design range used for the optimizer, and the maximum power was simply set by the maximum power that the fuel cell could deliver.

6. Uncertainties and limitations of this study

The (cyber-physical) simulation model includes components and subsystem models with varying accuracy. While the simulation on its own is performed with high accuracy, the abstractions in the model and the input parameters are partly very vague. This is especially the case for the fuel cell model; not so much on the (power and efficiency) but on the resulting size, weight and complexity of a fuel cell installation, including the necessary auxiliary systems such as fuel cell pressurization, humidification and especially the cooling system, which not only adds weight but also adds drag (and therewith lowers the L/D ratio of the aircraft). Therefore, there is a considerable uncertainty regarding the specific power (W/kg) and efficiency of the total fuel cell system installation on an aircraft. It is dealt here by just testing with different specific power. The power losses that comes form the auxiliary systems is not included and is probably significant. However, a model for this could easily be incorporated for this once available. The effect is however, quite straightforward. If the parasitic losses of the fuel cell is 10% it would mean that the hydrogen storage need to increase with about the same amount, thus reducing the payload capacity accordingly.

High uncertainties (due to the low TRL for aviation applications) are also on the hydrogen storage, but here experiences and values from automotive (namely the Toyota Mirai [13]) have been used, and the system is not as complicated as the fuel cell system. The *gravimetric index* (GI) (fuel fraction of total storage system weight) for high-pressure hydrogen tank of 6% for the pressurized hydrogen storage is based on the named automotive application. Significant higher values can be obtained with cryogenic liquid hydrogen (LH_2) tanks which are estimated to result in a GI of 0.2-0.35 [13]. As a comparison, rocket LH2 tanks reach GIs of ca. 0.85(!). From the aircraft design point of view, the often shown placement of the hydrogen fuel tank in the back of the fuselage imposes higher problems and (trim drag losses) due to CG changes during flight the higher the hydrogen storage GI is. However, for the limited ranges used here this is of no consequence since the change of hydrogen mass is less than would amount to corresponds to just one passenger. The size (around $1\mathrm{m}^2$) is also manageable. The largest uncertainty is not really technical, but related to the business case of this kind of aircraft. I.e., would a 19 passenger aircraft with this limited range be a viable proposition? However, regarding the size, it would scale fairly linearly with size. I.e. the weight fraction needed for energy storage and fuel cells would be roughly the same, although the aircraft would then fall into another set of regulations. There seems also to be a potential to increase the range even with a pressurized hydrogen storage, while maintaining a 19 passenger capacity within the weight limit.

Redundancy and Reliability

This study did not specifically investigate the system configurations with respect to reliability and redundancy. However, beside system acquisition, maintenance, and fuel costs, this is the major system architecture driver of manned aircraft propulsion systems. While the simulation model makes use of one fuel cell for simplicity (see Fig. 1), a real setup may be based on at least two independent fuel cells for redundancy reason. In case a design with only one hydrogen tank can be realized (violating the "single failure" rule), the battery may be seen as an alternative power source (under a limited time) to fulfil at least the requirement for two independent power sources under take-off and initial climb. From this perspective, the battery may be left in the design even though in the cases the fuel cell has a higher power density than a battery. Also, one has to make sure that the battery is (completely) recharged during the mission prior landing (a problem is missed approach and subsequent approach without longer loiter/cruise segment in between).

7. Discussion

Regarding the concept optimization, there are several factors that are balanced against each other. A battery assisted take-off and climb is attractive if the discharge time is sufficiently long. I.e. the climb in this example is about 16 minutes which means that the average discharge is about $16/60 \approx 3.7$. which means that the discharge rate is about $3.7C$, i.e 3.7 the capacity of the battery in Wh. Since the battery should not be fully depleted (in the optimization it is limited to a state of charge to about $SOC = 0.2$. This reduce the average discharge rate to about $3C$. This is reasonable and should be considered as acceptable with respect to excessive battery degradation. However, for a lower cruise altitude the discharge time would be reduced and therefore the battery could not be reduced to the corresponding degree.

However, a fuel cell with an over capacity for the cruise segment will also have a higher efficiency due to the characteristics of the fuel cell, and that will result in a reduced fuel consumption that to some degree can offset the increased fuel cell weight especially for long ranges. Therefore the size of the battery can change dramatically depending on the initial assumptions regarding parameters for the optimization. However, the consequences on the overall weight is quite marginal and secondary aspects not considered in this study might be more important (e.g. safety and redundancy).

It should be noted that the aircraft concept studied here was straightforward, with a two-engine configuration. However, increasing the number of motors or changing the concept of the aircraft can change the characteristics of the airplane. However, it is only the effect on the lift-to-drag (L/D) ratio and the propulsive efficiency that will have any influence on range. I.e, an increase of 10% of the lift-to-drag ratio (which is a lot), would just increase the range by the same amount, and the same goes for propulsive technology. The structural efficiency can be translated into an increase in payload or battery mass with the (CS/FAR 23) weight limit active. The energy carrier, on the other hand, have a huge impact and is therefore the focus of this study, and the optimization problem has here been set up to make this as decoupled as possible from the rest of the design.

8. Conclusion

In this paper two different missions and two different technology levels was studied. Since the models includes the possibility for both battery and fuel cells as power source, as well as a combination of both, an optimizer will find the optimal configuration. The results show that with the present level of technology, a combination of battery and fuel cell (battery assisted take-off and climb) seems optimal, at least for the short range aircraft. Looking at future higher specific power and energies of the components, and also varying aircraft range and payload requirements, other combinations may be favoured, including a pure battery powered aircraft for short ranges.

The paper also shows the use-fullness of the simulation based optimization approach. By including different possible combinations of solutions in a model, it is also possible to use it for concept optimization. Furthermore, the simulation model can also be used for other studies, i.e. performance and flight dynamics.

Acknowledgements

This paper has partly been supported by the Swedish National Research Program (NFFP), VINNOVA grant nr. 2018-00063.

Contact Author Email Address

Please contact the author at petter.krus@liu.se

References

[1] M. A. Al-Baghdadi and H. A. Al-Janabi. Optimization study of proton exchange membrane fuel cell performance. *Turkish Journal of Engineering and Environmental Sciences*, 29(4):235–240, 2005.

[2] C. Boccaletti, G. Duni, G. Fabbri, and E. Santini. Simulation models of fuel cell systems. *Proc. ICEM, Electrical Machines, Chania, Greece*, (September):6, 2006.

[3] EPE/MME/Brazil. Baseline to support the brazilian hydrogen strategy - epe-dea-nt-003/2021 rev01. Technical report, Energy Research Company - EPE, 2021.

[4] B. Eriksson, P. Nordin, and P. Krus. Hopsan NG, a C++ implementation using the TLM simulation technique. In *Conference of Scandinavian Simulation Society, sims' 10, 14th–15th October, Oulu, Finland*, 2010.

[5] IEA. Iea, irena, unsd, world bank, who. 2022. tracking sdg 7: The energy progress report. Technical report, World Bank, 2022.

[6] A. T. Isikveren, M. Bradley, B. Vite, R. Jansen, K. Papathakis, J. Tai, M. Patterson, J. Gladin, B. Schiltgen, R. Vos, P. Ansell, S. Clarke, N. Garrigan, G. Welch, R. Ouellette, K. Haran, and H. Schlickenmaier. Guidelines for analysis of hybrid electric aircraftsystem studies: Nomenclature, pictographic representations, standalone and combined properties and attributes, metrics, and figures of merit. Technical report, The American Institute of Aeronautics and Astronautics (AIAA), 2019.

[7] T. Kadyk, R. Schenkendorf, S. Hawner, B. Yildiz, and U. Römer. Design of fuel cell systems for aviation: Representative mission profiles and sensitivity analyses. *Frontiers in Energy Research*, 7(APR), 2019.

[8] P. Krus. Information Entropy in the Design Process. In *International Conference on Research into Design, ICoRD'13, 7th–9th January, Chennai, India*, 2013.

[9] P. Krus, R. Braun, and P. Nordin. Aircraft System Simulation for Preliminary Design. In *28th International Congress of the Aeronautical Sciences*, Brisbane, 2012. ICAS.

[10] P. Krus, A. Jansson, and J.-O. Palmberg. Optimization Using Simulation for Aircraft Hydraulic System Design. In *Procedings of IMECH International Conference on Aircraft Hydraulics and Systems*, number January 1993, London, U.K., 1993.

[11] J. Larmine and A. Dicks. *Fuel Cell Systems Explained*. Wiley, second edition, 2003.

[12] D. L. Marino, R. F. Figueroa, L. E. Garcia Acevedo, G. O. Porras, and A. A. M. Oliveira. Thermal and electrical characterization and modelling of a Proton Exchange Membrane Fuel Cell (PEMFC). Technical report, LABCET-UFSC, 2012.

[13] J. Mukhopadhaya and D. Rutherford. Performance Analysis Of Evolutionary Hydrogen-Powered Aircraft. Technical Report January, 2022.

[14] A. Omran, A. Lucchesi, D. Smith, A. Alaswad, A. Amiri, T. Wilberforce, J. R. Sodré, and A.G.Olabi. Mathematical model of a proton-exchange membrane (PEM) fuel cell. *International Journal of Thermofluids*, 11, 2021.

[15] H. Radmanesh, S. S. Heidari Yazdi, G. B. Gharehpetian, and S. H. Fathi. Modelling and simulation of fuel cell dynamics for electrical energy usage of Hercules airplanes. *The Scientific World Journal*, 2014, 2014.

[16] I. Staack, A. Sobron, and P. Krus. The potential of full-electric aircraft for civil transportation: from the Breguet range equation to operational aspects. *CEAS Aeronautical Journal*, 12(4):803–819, 2021.